Functional and Structural Interactions of the Transmembrane Domain X of NhaA, Na^+/H^+ Antiporter of *Escherichia coli*, at Physiological pH†

Lena Kozachkov, Katia Herz, and Etana Padan*

Alexander Silberman Institute of Life Sciences, Hebrew University of Jerusalem, Jerusalem 91904, Israel

Received November 20, 2006; Revised Manuscript Received December 24, 2006

ABSTRACT: The 3D structure of *Escherichia coli* NhaA, determined at pH 4, provided the first structural insights into the mechanism of antiport and pH regulation of a Na^+/H^+ antiporter. However, because NhaA is activated at physiological pH (pH 7.0−8.5), many questions pertaining to the active state of NhaA have remained open, including the physiological role of helix X. Using a structural-based evolutionary approach *in silico*, we identified a segment of most conserved residues in the middle of helix X. These residues were then used as targets for functional studies at physiological pH. Cysteine-scanning mutagenesis showed that Gly303, in the middle of the conserved segment, is an essential residue and Cys replacement of Lys300 retains only Li^+/H^+ antiporter activity, with a 20-fold increase in the apparent K_M for Li^+. Cys replacements of Leu296 and Gly299 increase the apparent K_M of the Na^+/H^+ antiporter for both Na^+ and Li^+. Accessibility test to *N*-ethylmaleimide and 2-sulfonatoethyl methanethiosulfonate showed that G299C, K300C, and G303C are accessible to the cytoplasm. Suppressor mutations and site-directed chemical cross-linking identified a functional and/or structural interaction between helix X (G295C) and helix IVp (A130C). While these results were in accordance with the acid-locked crystal structure, surprisingly, conflicting data were also obtained; E78C of helix II cross-links very efficiently with several Cys replacements of helix X, and E78K/K300E is a suppressor mutation of K300E. These results reveal that, at alkaline pH, the distance between the conserved center of helix X and E78 of helix II is drastically decreased, implying a pH-induced conformational change of one or both helices.

Sodium-proton antiporters are ubiquitous membrane proteins found in the cytoplasmic and organelle membranes of cells of many different origins, including plants, animals, and microorganisms. They are involved in cell energetics and play primary roles in the regulation of intracellular pH, cellular Na^+ content, and cell volume (recent reviews in refs *1*−*3*). These basic and essential physiological roles explain why an alternation in activity of certain antiporters has a huge impact on cell viability.

Ec-NhaA,[1] the main Na^+/H^+ antiporter of *Escherichia coli* (if not otherwise stated, henceforth, NhaA), is indispensable for adaptation to high salinity, challenging Li^+ toxicity, and growth at alkaline pH [in the presence of Na^+ (*3*, *4*)]. It is widely spread in enterobacteria (*1*) and has orthologues throughout the biological kingdom, including humans (*5*).

NhaA is dramatically dependent upon pH. Its rate of activity changes over 3 orders of magnitude between pH 7.0 and 8.5 (*2*, *3*, *6*). This change is accompanied by a conformational alternation, as probed by a monoclonal antibody (*7*), accessibility of NhaA to trypsin (*8*), or 2-(4′-maleimidylanilino)-naphthalene-6-sulfonic acid (MIANS), a fluorescent probe (*9*). Similarly, many of the eukaryotic (*10*−*12*) and prokaryotic (*3*, *6*) Na^+/H^+ antiporters are controlled by pH, a property that underpins their function in pH homeostasis (*3*).

The recently determined crystal structure of the acidic down-regulated NhaA at pH 4 (*13*) has provided the first structural insights into the mechanism of antiport and pH regulation of a Na^+/H^+ antiporter. The structure shows that NhaA consists of 12 transmembrane segments (TMSs), with the N and C termini pointing into the cytoplasm, in line with previous biochemical (*14*) and genetic (*15*) results. The structure represents a novel fold; helices IV and XI unwind in the middle of the membrane to form two pairs of short helices IVp, IVc, XIp, and XIc (p and c stand for periplasmatic and cytoplasmatic, respectively) connected by extended chains that cross each other in close contact in the middle of the membrane [TMSs IV/XI assembly (*13*) and Figure 1]. This creates a delicately balanced electrostatic environment in the middle of the membrane. Combining the structural data obtained at pH 4 with the biochemical (*16*), genetic (*17*, *18*), and biophysical (*9*) data obtained at physiological pH at which NhaA is activated (pH 7.0−8.5) allowed us to build a working model for the mechanism of activity and pH regulation of NhaA (*13*).

† This research was supported by a grant from the German−Israeli Foundation (GIF) for Scientific Research and Development (to E.P.), the Israel Science Foundation (501/03-16.2), and the U.S.A.−Israel Binational Science Foundation (BSF).

* To whom correspondence should be addressed. Telephone: 972-2-6585094. Fax: 972-2-6586947. E-mail: etana@vms.huji.ac.il.

[1] Abbreviations: TMS, transmembrane segment; Ec-NhaA, *E. coli* NhaA; Hp-NhaA, *H. pylori* NhaA; CL-NhaA, cysteine-less NhaA; NEM, *N*-ethylmaleimide; BMH, 1,6-*bis*-maleimidohexane; *o*-PDM, *N*,*N*′-*ortho*-phenylenedimaleimide; MTS-2-MTS, 1,2-ethanediyl bismethanethiosulfonate; BTP, 1,3-*bis*-{tris(hydroxymethyl)-methylamino} propane; DTT, dithio-D,L-threitol; MTSES, 2-sulfonatoethyl methanethiosulfonate; MIANS, 2-(4′-maleimidylanilino)-naphthalene-6-sulfonic acid; DMF, dimethylformamide.

10.1021/bi602393s CCC: $37.00
Published on Web 02/07/2007

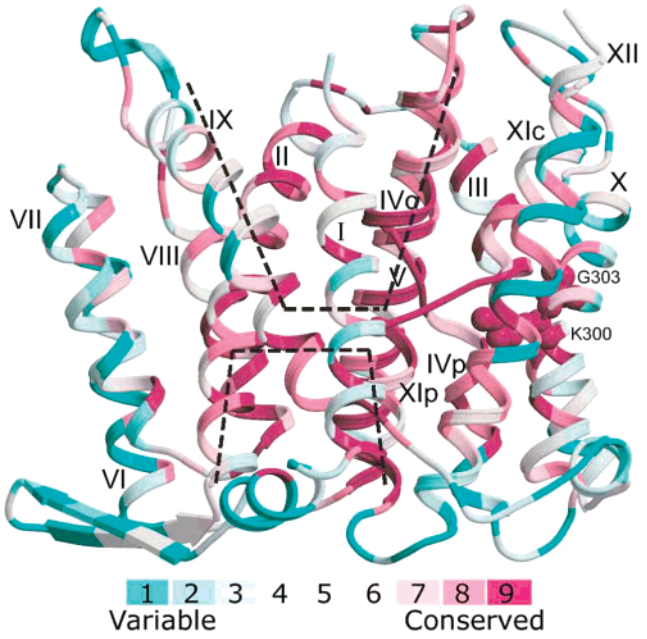

FIGURE 1: ConSurf analysis of NhaA. The *in silico* analysis [http:/consurf.tau.ac.il (*24*)] was carried out using PDB entry code 1ZCD (*13*) and a multiple sequence alignment of 100 homologue sequences from the Na^+/H^+ antiporter family, taken from the Pfam database (*25*). NhaA is viewed parallel to the membrane as a ribbon representation. The TMS are numbered. K300 and G303 (TMS X) are represented by balls. The amino acids are colored by their conservation grades using the color-coding bar, with turquoise−maroon indicating variable−conserved. The picture was generated using MOLSCRIPT (*46*) and Raster3D (*47*). The cytoplasmic (upper) and periplasmic (lower) funnels are indicated by a dashed line.

A negatively charged ion funnel opens to the cytoplasm and acts as a cation trap. It ends in the middle of the membrane in the vicinity of the ion-binding site and the crossing of the TMSs IV/XI assembly. A pH sensor perceives a pH signal at the orifice of the cytoplasmic funnel and transfers the signal to the TMSs IV/XI assembly, modifying its conformation, in a pH-dependent manner, to activate the ion-exchange mechanism.

The structure shows that K300 of TMS X plays a highly crucial role in the unique architecture of the acid-locked conformation of NhaA; it compensates the negative dipoles of the opposing helices XIc and IVp in the middle of the membrane (see ref *13* and Figures 1 and 2b). This contributes to the delicately balanced electrostatic environment in the core of the membrane that has been assigned a crucial role in the transport mechanism of NhaA and its regulation by pH. However, the role of helix X in the functionality of NhaA has not yet been studied at physiological pH, when NhaA is pH-activated. Therefore, many questions pertaining to the active state of NhaA have remained open: Are K300 and/or other amino acid residues in helix X crucial for the activity of NhaA? Are those residues involved in the pH regulation of the antiporter? Do residues in helix X change conformation with pH?

To answer these questions, we first applied a structural-based evolutionary approach in which conserved residues were identified and their conservation grades were projected on the NhaA structure (Figure 1). In this way, a patch of the evolutionary most conserved amino acid sequence was identified in the middle of TMS X, facing the cytoplasmic funnel (parts b and c of Figure 2). These conserved residues then served as targets for Cys replacements and the study of the effect of the mutations on growth (in the presence of high Na^+ or Li^+) and antiporter activity in isolated membrane vesicles. The Cys replacements were tested for accessibility to both sides of the membrane and their interactions with other TMSs in the molecule. All of these experiments were conducted at the physiological pH range when NhaA is active.

The data presented here show that residues in the middle of the conserved patch of helix X play an important physiological role in the translocation mechanism of NhaA. Furthermore, at physiological pH, as at acidic pH, helix IVp interacts structurally and/or functionally with the C-terminal half of TMS X. However, surprisingly, at alkaline pH, the distance between the most conserved segment, in the middle of helix X, and E78 of helix II decreases, implying a pH-induced conformational change in one or both helices.

MATERIALS AND METHODS

Bacterial Strains and Culture Conditions. EP432 is an *Escherichia coli* K-12 derivative, which is *mel*BLid, Δ*nha*A1::*kan*, Δ*nha*B1::*cat*, Δ*lac*ZY, *thr1* (*19*). TA16 is *nha*A^+*nha*B^+-*lac*I^Q (TA15*lac*I^Q) and otherwise isogenic to EP432 (*6*). Cells were grown in either L broth (LB) or modified L broth [LBK (*4*)]. Where indicated, 60 mM 1,3-*bis*-{tris(hydroxymethyl)-methylamino} propane (BTP) was added. Cells were also grown in minimal medium A without sodium citrate (*20*) with 0.5% glycerol, 0.01% $MgS0_4 \cdot 7H_20$, and thiamine (2.5 μg/mL). For plates, 1.5% agar was used. Antibiotics were 100 μg/mL ampicillin and/or 50 μg/mL kanamycin. The resistance to Li^+ and Na^+ was tested as previously described (*4*).

Plasmids. Plasmid pGM36 encodes NhaA (*21*). pCL-GMAR100, a derivative of pGM36, encodes Cys-less NhaA [CL-NhaA, (*14*, *22*)]. pECO, a derivative of pGMAR100 (with an *Eco*RI site at position 5319), encodes NhaA (*16*). pAXH (previously called pYG10), a pET20b (Novagen) derivative, encodes His-tagged NhaA (*14*). pCL-AXH, a derivative of pAXH, encodes a His-tagged CL-NhaA (*14*). pCL-AXH2, a derivative of pCL-AXH, lacks a *Bgl*II site at position 3382 (*16*). pCL-AXH3, a derivative of pCL-AXH2, contains a *Bst*XI silent site at position 248 in *nha*A. pCL-HAH4, a derivative of pCL-HAH3, bears a silent *Bst*XI mutation and encodes His-tagged CL-NhaA (*23*). All plasmids carrying mutations are designated by the name of the plasmid followed by the mutation.

ConSurf Analysis of NhaA. The ConSurf web-server [http:/consurf.tau.ac.il (*24*)] analysis allowed projecting evolutionary conservation scores of amino acid residues on the NhaA protein structure. This *in silico* analysis is most interesting because structurally and/or functionally important regions typically appear as patches of evolutionary-conserved residues that are spatially close to each other in the protein. The analysis was carried out using Protein Data Bank (PDB) entry code 1ZCD (*13*) and a multiple sequence alignment of 100 homologue sequences from the Na^+/H^+ antiporter family, taken from the Pfam database (*25*).

Site-Directed Mutagenesis. Site-directed mutagenesis was conducted following a polymerase chain reaction (PCR)-

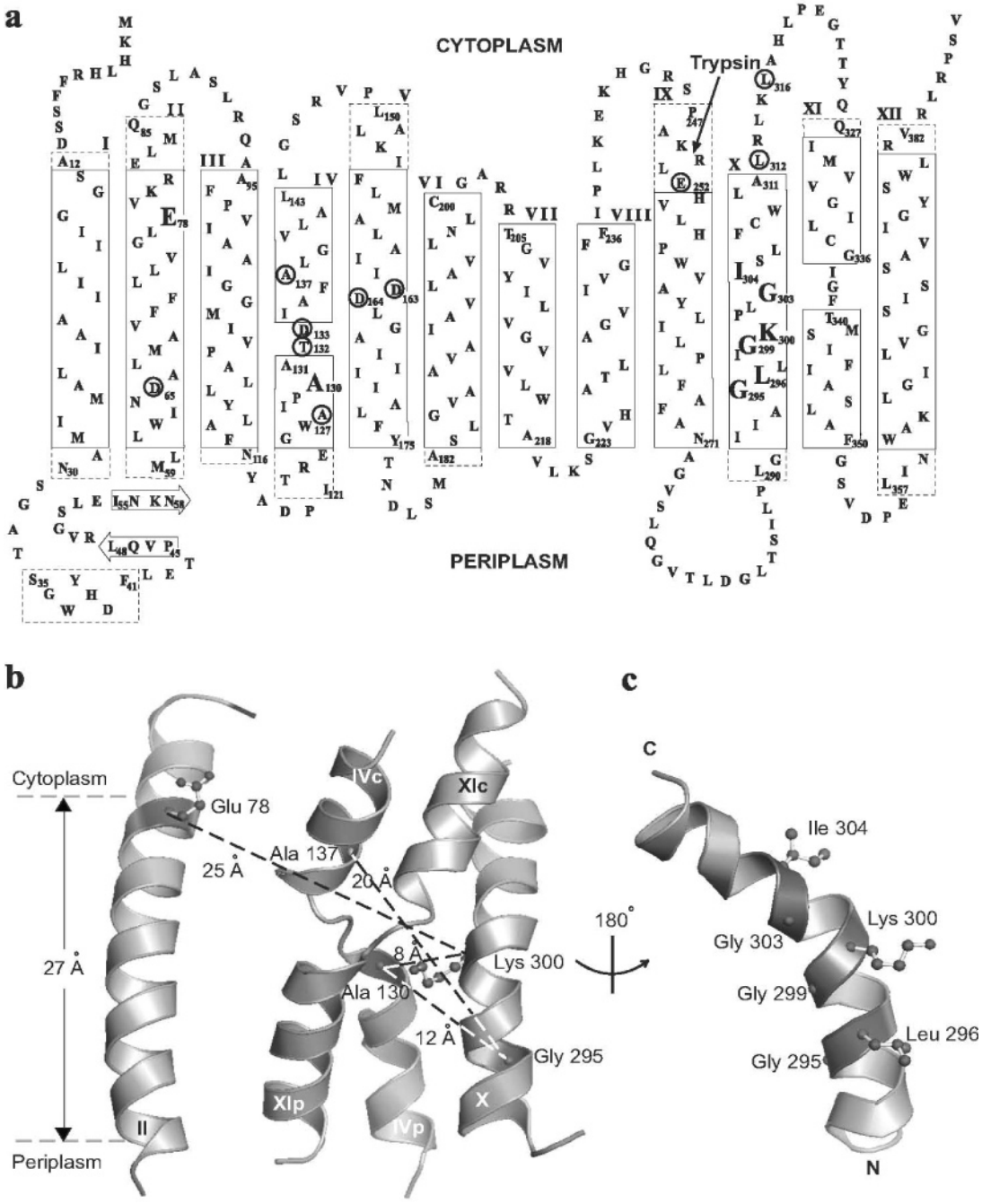

FIGURE 2: Topology model of NhaA showing (a) the mutated residues, (b) the unique position of TMS X in the structure of NhaA, and (c) its conserved face. (a) The 12 TMS topology model of NhaA is shown based on the 3D structure (*13*). The single-letter amino acid code is used, and the location in the amino acid sequence is indicated by a number. The Roman numerals indicate the numbers of the TMS shown by rectangles. The membrane-embedded regions of the TMSs are designated by a continuous line, and the regions of the TMSs exposed to the cytoplasm or periplasm are designated by a broken line. The arrow-like boxes show the antiparallel β-sheet element. Enlarged letters indicate residues mutated in this work, and encircled letters designate previously mutated residues that were used in this work. (b and c) All of the distances were calculated between α carbons of the respective residues in the NhaA structure (*13*). N and C indicate the amino and carboxy termini of the TMS, respectively. The ribbon representation viewed parallel to the membrane (gray broken lines) was generated using PyMOL (http://pymol.sourceforge.net/).

based protocol (*26*) or *Dpn*I-mediated site-directed mutagenesis (*27*).

For Cys replacement of E78, G295, L296, G299, K300, G303, and I304, pCL-HAH4 was used as a template. For Cys replacement of A130, pCL-AXH was used as a template. For construction of E78K and K300E, pCL-AXH3 and pAXH were used as templates, respectively. All of the mutagenic primers are described in Table 1, and the mutations are marked on the new topology model of NhaA (Figure 2a).

Mutations in TMS IV (A127C, T132C, D133C, and A137C) have been previously described (*16*, *17*, *28*). Double mutants in TMSs II/X and IV/X were obtained by ligating the *Eco*RI−*Bgl*II fragment (465 bp) of the single-Cys NhaA mutant in TMS II or IV with the *Eco*RI−*Bgl*II fragment (4.28 kb) of the plasmid, encoding the respective single-Cys NhaA

Table 1: Oligonucleotides Used for Constructing the Cys Mutations in *nha*[a]

silent restriction site	codon change	primer sequence	mutation
*Eco*31I	GAA to TGT	GTCGGTCTC*__TGT__GTTAAACG	E78C
*Eco*31I	GAA to AAA	CGGTCTC*__AAA__GTTAAACG	E78K
*Fsp*I	GCG to TGC	CGATCCCG__TGC__GCA*ACTGACATTGC	A130C
*Pae*I	GGC to TGC	GGGATCATCGCA*__T__GCTTGCTGAATGGC	G295C
*Bgl*I	TTG to TGC	CATCGCTGGCT__GC__CTGATTGGC	L296C
*Nde*I	GGC to TGC	GGCTTGCTC*ATA*__T__GCAAACCGCTGGGG	G299C
*Mbi*I	AAA to TGC	GGCTTGCTGATTGGC__TGC__CCGCTC*GGG	K300C
*Eco*24I	AAA to GAG	GCTGATTGGC__GAG__CCC*CTGGGG	K300E
*Mph*1103I	GGG to TGC	GGCAAACCGCTA*__T__GC__A__TTAGTCTG	G303C
*Pst*I	ATT to TGC	ACCGCTGGGC*__TGC__AGTCTGTTC	I304C
none	none	sense primer TTTAACGATGATTCGTGGCGG antisense primer GCTCATTTCTCTCCCTGATAAC	end primers for mutations E78C and A130C

[a] The mutated bases are shown in bold. Additional substitutions (*) have been introduced to create silent mutations as indicated.

mutant in TMS X. All mutations were verified by DNA sequencing of the entire gene, through the ligation junction with the vector plasmid.

Random Mutagenesis. Random mutagenesis was conducted *in vitro* by hydroxylamine hydrochloride as described (*18*) or PCR as described (*29*) on plasmids pGM36 and pECO encoding mutants K300C and G303C, respectively. The mutated plasmids were transformed into the EP432 strain, and *nha*A mutants that grew on selective agar plates (LBK medium containing 0.6 M Na^+ at pH 7.0 or 8.3 or 0.2 M Li^+ at pH 7.0) were isolated.

Isolation of Membrane Vesicles, Assay of $Na^+(Li^+)/H^+$ Antiport Activity. EP432 cells transformed with the respective plasmids were grown, and everted vesicles were prepared and used to determine the Na^+/H^+ or Li^+/H^+ antiport activity as described (*30*, *31*). The assay of antiport activity was based on the measurement of Na^+- or Li^+-induced changes in the ΔpH as measured by acridine orange, a fluorescent probe of ΔpH. The fluorescence assay was performed with 2.5 mL of reaction mixture containing 50−100 μg of membrane protein, 0.5 μM acridine orange, 150 mM KCl, 50 mM BTP, and 5 mM $MgCl_2$, and the pH was titrated with HCl. After energization (downward-facing arrow in Figure 3a) with either ATP (2 mM) or D-lactate (2 mM), quenching of the fluorescence was allowed to achieve a steady state and then either Na^+ or Li^+ was added (upward-facing arrow in Figure 3a). A reversal of the fluorescence level (dequenching) indicates that protons are exiting the vesicles in antiport with either Na^+ or Li^+ as indicated. As shown previously, the end level of dequenching is a good estimate of the antiport activity (*32*) and the concentration of the ion that gives half-maximal dequenching is a good estimate of the apparent K_M of the antiporter (*32*, *33*). The concentration range of the cations tested was 0.01−100 mM at the indicated pH values, and the apparent K_M values were calculated by linear regression of a Lineweaver−Burk plot.

Detection and Quantization of NhaA and Its Mutated Proteins in the Membrane. NhaA and its mutated derivatives were quantitated by Western analysis using an anti-NhaA monoclonal antibody 1F6 (*34*), as described previously (*35*). The total membrane protein was determined according to ref *36*. The expression level of His-tagged NhaA mutants was determined by resolving the Ni−nitrilotriacetic acid (NTA)-purified proteins on sodium dodecyl sulfate−polyacrylamide gel electrophoresis (SDS−PAGE), staining the gels by Coomassie blue, and quantization of the band densities (*14*).

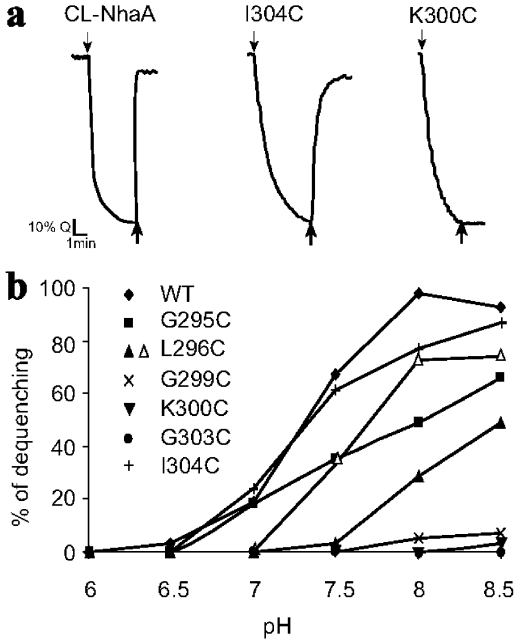

FIGURE 3: Na^+/H^+ antiport activity in everted membrane vesicles of single NhaA mutants in TMS X. Everted membrane vesicles were prepared from EP432 cells expressing the indicated NhaA mutants and grown in LBK (pH 7). (a) Na^+/H^+ antiport activity was measured at pH 8.5. The data of typical experiments are shown. At the onset of the reaction, Tris D-lactate (2 mM) was added (↓) and the fluorescent quenching (*Q*) was recorded until a steady-state level of ΔpH (100% quenching) was reached. NaCl or LiCl, at the indicated concentrations, was then added (↑), and the new steady state of fluorescence obtained (dequenching) after each addition was monitored. (b) Na^+/H^+ antiport activity was determined at the indicated pH values as described above in the presence of 10 mM NaCl (closed symbols) or 100 mM NaCl (open symbols). For more details, see the Materials and Methods. The results are expressed as the end level of dequenching (%). All experiments were repeated at least 3 times with practically identical results.

Determination of Accessibility to N-Ethylmaleimide (NEM). TA16 cells were transformed with *nha*A mutants expressing plasmids. The preparation of membrane vesicles was carried out as described above but with no dithio-D,L-threitol (DTT) in the resuspension medium. The membrane vesicles (200 μg) were resuspended in 500 μL containing 100 mM potassium phosphate at pH 7.5 and 5 mM $MgSO_4$. Membranes were treated with 0.5 mM [^{14}C]NEM (specific activity

of 4 μCi/μmol), and the NEM-alkylated residues were quantitated as a percentage of the control after normalization by the amount of the protein, as described (*14*). The standard deviation was between 5 and 10%.

Accessibility to Impermeable Sulfhydryl Reagent [2-Sulfonatoethyl methanethiosulfonate (MTSES)] in Intact Cells and Everted Vesicles. The accessibility in intact cells was performed as described (*37*), but the Tris buffer was replaced with 100 mM potassium phosphate and 5 mM $MgSO_4$ (pH 7.4). For accessibility to MTSES from the cytoplasmic side, everted membrane vesicles (300 μg of membrane protein) were incubated with 10 mM MTSES, at room temperature with gentle shaking for 10 min. Then, the membranes were centrifuged (Beckman, TLA 100.4, 265000*g* for 20 min at 4 °C) and washed in potassium buffer, and the protein was affinity-purified on Ni−NTA and subjected to fluorescine maleimide to determine the free Cys left, as described (*23*). The standard deviation was between 5 and 10%.

In Situ Site-Directed Inter and Intramolecular Cross-Linking. Site-directed intramolecular cross-linking was conducted *in situ* on membrane vesicles isolated from TA16 cells expressing the various NhaA double mutants. Membranes (3 mg of protein) were resuspended in a buffer (4.5 mL) containing 100 mM potassium phosphate, 5 mM $MgSO_4$ (pH 7.4), and one of the freshly prepared homo-bifunctional cross-linkers: 2 mM 1,6-*bis*-maleimidohexane (BMH) (Pierce), 1 mM *N*,*N*′-*ortho*-phenylenedimaleimide (*o*-PDM) (Sigma), or 2 mM 1,2-ethanediyl bismethanethiosulfonate (MTS-2-MTS) (Toronto Research Chemicals). The stock solutions of the cross-linkers were prepared in dimethylformamide (DMF) at 200 mM, so that the amount of DMF in the reaction mixture did not exceed 1%, a concentration that did not affect the antiporter activity. The suspension was incubated at 26 °C with gentle rotation for 60 min. The reaction with BMH or *o*-PDM was terminated by the addition of 10 mM β-mercaptoethanol, and the reaction with MTS-2-MTS was terminated by dilution (14-fold) and centrifugation (Beckman, MLA-80, 265000*g* for 20 min at 4 °C). The protein was Ni−NTA-affinity-purified, treated with trypsin at alkaline pH, and separated on SDS−PAGE (nonreducing conditions in the case of treatment with MTS-2-MTS) to identify the proteolytic products according to ref *23*. Because the only trypsin-cleavable site (K249) is located between TMS II or IV and TMS X (Figure 2a), trypsinolysis of untreated samples results in two tryptic peptides of mobility faster than the intact protein (17, 24, and 32.5 kDa, respectively). On the other hand, intramolecular cross-linking results in one fragment of mobility equal to that of the intact protein (*23*). Each experiment was repeated at least twice with practically identical results.

In situ site-directed intermolecular cross-linking between NhaA containing single-Cys replacements was tested as above but without treatment with trypsin. When intermolecular cross-linking takes place, a band, corresponding in mobility to that of the NhaA dimer, appears in SDS−PAGE (*22*, *23*).

RESULTS

Projection of Evolutionary-Conserved Residues on the NhaA Structure. The structure of the acid-locked conformation of NhaA (*13*) has revealed that K300 of TMS X is located in a unique position in the middle of the membrane, where it compensates the negative dipoles of the opposing short helices XIc and IVp of the TMSs IV/XI assembly of NhaA (see ref *13* and Figures 1 and 2b). This contributes to the delicately balanced electrostatic environment in the middle of the membrane that has been assigned a crucial role in the translocation mechanism of NhaA. The first aim of the presented work was to identify amino acid residues in TMS X that play a role in the cation-exchange activity of NhaA and/or its pH regulation. Our functional analysis was conducted at the physiological pH range, activating NhaA (pH 7.0−8.5), in contrast to pH 4, where the NhaA crystals were obtained. Therefore, confronting our functional data with the acid-locked structure also allowed us to deduce pH-induced conformational changes.

The high level of evolutionary conservation often corresponds to the functionally and/or structurally important sites of the protein. Therefore, to guide our functional analysis of TMS X, we applied an approach that combined the crystallographic data with an evolutionary-oriented *in silico* method (Figure 1). First, the NhaA protein sequence was aligned with 100 prokaryotic homologue sequences from the Na^+/H^+ antiporter family, taken from the Pfam database (*25*). Then, the evolutionary conservation scores of the amino acids in NhaA were projected on the 3D structure of the protein, using the ConSurf web server [http:/consurf.tau.ac.il (*24*)]. The ConSurf analysis of the NhaA crystal structure shows that, remarkably, the large part of the core of the TMSs IV/XI assembly, where the extended chains cross, is the most evolutionarily conserved. Furthermore, highly conserved patches of amino acids cluster in the middle of TMSs V and X, facing the crossing of the TMSs IV/XI assembly (Figure 1).

The evolutionary-conserved segment in the middle of TMS X is the focus of the present work. It is localized on one face of the helix (parts b and c of Figure 2) and comprised, at its center, of residues (G299, K300, and G303) that are 100% conserved and, at both of its ends, of residues (G295, L296, and I304) that are replaceable in a conservative fashion (Figures 1 and 2c).

Cys-Replacement Mutations of the Conserved Residues in TMS X, Expression in the Membrane, and Growth Phenotypes at Physiological pH. Because almost no biochemical and genetic studies have been conducted to explore the functional importance of helix X of NhaA, we constructed Cys-replacement mutations of the highly conserved amino acid residues in helix X (parts a and c of Figure 2 and Table 1). If not otherwise stated, all mutants were constructed in CL-NhaA, a variant that is as expressed and active as the native NhaA (*14*). The mutations were subjected to functional studies at physiological pH (pH 7.0−8.5), which progressively activates NhaA (*2*, *6*).

To characterize the mutations with respect to expression, growth, and antiport activity (Table 2 and Figure 3), the mutated plasmids were transformed into EP432, an *E. coli* strain that lacks the two Na^+-specific antiporters (NhaA and NhaB). This strain neither grows on selective media (0.6 M NaCl at pH 7.0 or 8.3 or 0.2 M LiCl at pH 7.0) nor exhibits any Na^+/H^+ antiport activity in isolated everted membrane vesicles, unless transformed with a plasmid encoding an active antiporter (reviewed in refs *1* and *3*).

Table 2: Single-Cys Replacements of Conserved Residues in TMS II, IV, and X of NhaA[a]

		growth			activity (max. dequenching %)		apparent K_M (mM)	
mutation	expression	Na^+ (7)	Na^+ (8.3)	Li^+ (7)	Na^+	Li^+	Na^+	Li^+
TMS II								
E78C	20	+++	+++	+++	69	100	0.4	0.04
E78K	15	+++	+++	+++	ND	ND[b]	ND	
TMS IV								
A130V	ND	+++	+++	+++	71	100	0.4	0.02
A130C	ND	+++	+++	+++	92	100	0.4	0.03
D133C	10	+++	+++	+++	87	70	3.6	1.24
TMS X								
G295C	88	+++	+++	+++	70	91	2	0.98
L296C	100	+++	+	+++	52	100	10.1	0.29
G299C	67	+++	−	+++	7	42	27	1.53
K300C	50	−	−	−	0	44	ND	4
K300E	15	−	−	−	ND	ND	ND	ND
G303C	22	−	−	−	0	0	ND	ND
I304C	78	+++	+++	+++	93	98	0.7	0.1
controls								
pCL-HAH4	100	+++	+++	+++	100	100	0.8	0.2
pBR322	−	−	−	−	−	−	−	−

[a] For characterization of the mutants, EP432 cells transformed with the plasmids carrying the indicated mutations were used. The expression level was expressed as a percentage of the control cells (EP432/pCL-HAH4). Growth experiments were conducted on agar plates with high Na^+ (0.6 M) or high Li^+ (0.2 M) at the pH values indicated in parentheses. (+++) The number and size of the colonies after 24 h of incubation at 37 °C was identical to that of the wild type. (+) The number of colonies was similar but much smaller than that of the wild type. (−) No growth. Na^+/H^+ and Li^+/H^+ antiport activity at pH 8.5 was determined with 10 mM NaCl or LiCl. The activity (maximal level of dequenching) is expressed as a percentage of the positive control, EP432/pCL-HAH4. EP432/pBR322 served as a negative control. The apparent K_M for the ions was determined at pH 8.5, as described under the Materials and Methods. The experiments were repeated 3 times with essentially identical results. [b] ND = not determined.

As compared to the level of expression of the control (100%), the Cys-replacement mutants G295C, L296C, G299C, K300C, and I304C were expressed to 50−100% and G303C was expressed to 22% (Table 2). All variants were expressed from multicopy plasmids, so that their proteins were readily detected by Western analysis. These expression levels are above that obtained from a single chromosomal gene that confers a wild-type phenotype (*35*).

The mutants K300C and G303C did not grow on the high Na^+- or Li^+-selective media (whether in the wild-type or Cys-less genetic background, data not shown and Table 2). The mutants G299C and L296C grew on high Na^+ or Li^+ at neutral pH similar to the wild type. However, at alkaline pH in the presence of Na^+, G299C did not grow, while L296C grew much slower than the wild type. Mutants G295C and I304C grew similar to the wild type on all selective media (Table 2).

Mutations in TMS X That Drastically Inhibit the Na^+/H^+ Antiporter Activity at Physiological pH. The Na^+/H^+ antiport activity was measured in everted membrane vesicles isolated from EP432 transformed with the plasmids encoding the various mutations. The activity was estimated from the change caused by Na^+ or Li^+ to the ΔpH maintained across the membrane, as measured by acridine orange, a fluorescent probe of ΔpH. After energization (downward-facing arrow in Figure 3a) with either ATP or D-lactate, quenching of the fluorescence achieved a steady state and then either Na^+ or Li^+ was added (upward-facing arrow in Figure 3a). A reversal of the fluorescence level (dequenching) indicates that protons are exiting the vesicles in antiport with either Na^+ or Li^+ as indicated (further details in the Materials and Methods). EP432 transformed with plasmid pCL-HAH4 encoding CL-NhaA or the vector plasmid, pBR322, served as positive (Figure 3a and Table 2) and negative controls, respectively (Table 2). The apparent K_M values for Na^+ and Li^+ at pH 8.5 and the extent of activity at pH 8.5 (maximal dequenching, Table 2) as well as the pH dependence of the extent of the Na^+/H^+ antiport activity (Figure 3) were determined for each mutant.

The mutants G303C and K300C did not show any Na^+/H^+ antiport activity (parts a and b of Figure 3 and Table 2). Mutations L296C and G299C reduced the extent of the Na^+/H^+ antiport activity (52 and 7% of the control level, respectively, Figure 3b and Table 2) and caused a drastic increase in the apparent K_M of the antiporter to Na^+ (13- and 34-fold, respectively). Mutations I304C and G295C had a very small effect on the kinetic parameters of NhaA (parts a and b of Figure 3 and Table 2).

Mutant G303C did not have any antiport activity, implying that G303 is an essential residue for the activity of NhaA. The other mutants had a significant Li^+/H^+ antiport activity (Table 2). However, K300C and G299C caused a pronounced increase in the apparent K_M for Li^+ (20- and 8-fold, respectively, Table 2).

We have previously shown (*16*, *17*) that mutations that affect the apparent K_M for the ions but not the pH dependence of NhaA show a pH dependence very similar to that of the wild type, when measured at saturating concentrations of the respective ions. In contrast, mutations that affect both the apparent K_M for the cations and the pH dependence of NhaA retain the abnormal pH dependence, even at saturating concentrations of the respective ions. We therefore measured the effect of Na^+ concentrations (10 versus 100 mM) on the pH dependence of the mutants and found that, at both the high and low Na^+ concentrations, the pH dependence of G295C and I304C was very similar to that of the wild-type

protein (Figure 3b and data not shown). At low Na^+ concentrations, the pH profile of L296C antiport activity was shifted to the basic pH (Figure 3b) but the pH shift was significantly decreased at the high Na^+ concentration (Figure 3b). The effect of increasing the Na^+ concentration on the very low exchange activity of G299C was impossible to accurately measure. We therefore suggest that the Cys-replacement mutations of TMS X mainly affect the ion translocation process and not the pH dependence of the NhaA antiporter.

Accessibility to NEM of the Cys-Replacement Mutations in TMS X at Physiological pH. The acid-locked crystal structure of NhaA shows that, at acidic pH, TMS X is not located in either the cytoplasmic or periplasmic funnels (see ref *13* and Figure 1). However, this does not exclude the possibility that at physiological pH the conserved patch of TMS X becomes accessible to either one or both funnels, directly or via water molecules. We tested whether the Cys replacements in helix X were accessible to chemical modification by NEM in isolated membrane vesicles, *in situ*, at physiological pH. NEM, a membrane-permeable SH reagent modifies Cys in proteins upon ionization of the Cys-sulfhydryl to its thiolate form. As a positive control, we used H225C that is efficiently labeled by [^{14}C]NEM (see ref *14* and Figure 4a). As a negative control, we used CL-NhaA that is not labeled by [^{14}C]NEM (data not shown and ref *14*). Mutants G295C, L296C, and I304C were not labeled by [^{14}C]NEM. In mark contrast, mutants G299C, K300C, and G303C were strongly labeled by [^{14}C]NEM (Figure 4a).

We next tested which of these residues is freely accessible from the periplasm and/or cytoplasm. For this purpose, we used MTSES, a negatively charged, water-soluble membrane-impermeable SH reagent (*38*, *39*). Accessibility of the NhaA variants to MTSES was determined from either side of the membrane using intact cells and everted membrane vesicles (*23*). The Cys replacements, H225C and E78C, served as positive controls that are accessible from either the periplasmic or cytoplasmic side of the membrane, respectively (see ref *14* and Figure 4b). The results showed that G299C, K300C, and G303C were accessible to MTSES in everted membrane vesicles (at least 40% of the control) but not in intact cells. The Cys-replacement G295C was slightly labeled by MTSES (20% of the control) from both sides of the membrane, while L296C and I304C were not accessible to MTSES from either side of the membrane. Note that G295C was not accessible to NEM while showing a low accessibility to MTSES (compare parts a and b of Figure 4). We do not know the reason for this discrepancy. It can be due to different stereochemistry of the reagents or a more sensitive fluorescent-based protocol used for MTSES. When the results are taken together, they show that G299C, K300C, and G303C are accessible to the cytoplasm.

Isolation of Second-Site Suppressor Mutations to K300C. The acid-locked structure of NhaA shows that, at acidic pH, TMS X is in close proximity to TMS IVp (Figure 2b). Assuming that similar proximity exists at physiological pH, second-site mutants in TMS IVp might suppress mutants in TMS X. Therefore, the plasmids carrying the NhaA mutations K300C and G303C were randomly (chemically or by PCR) mutagenized, transformed into EP432, and grown on agar plates containing either high Na^+ (pH 7.0 or 8.3) or high Li^+ (pH 7.0) selective media. K300C but not G303C

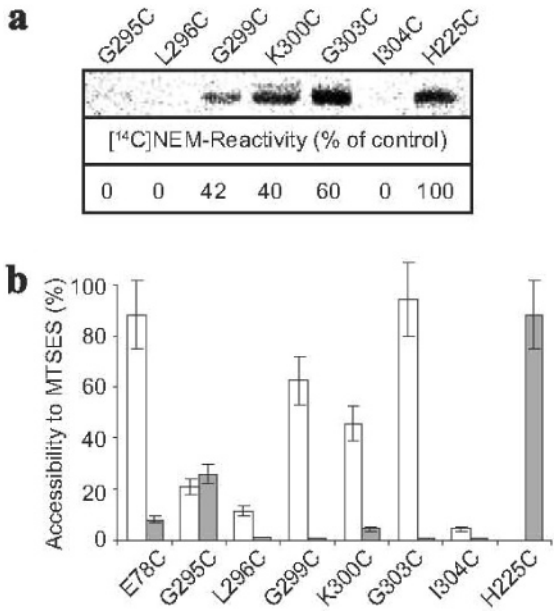

FIGURE 4: Accessibility of Cys replacements in TMS X to NEM and MTSES. Membrane vesicles were prepared from cells expressing the Cys-replacement mutants in TMS X of Cys-less NhaA. (a) Membrane vesicles (200 μg of protein) were incubated with [^{14}C]-NEM as described in the Materials and Methods. The membranes were washed and solubilized, and after affinity purification, the protein was resolved on SDS−PAGE, stained by Coomassie blue, and scanned to estimate the amount of protein for normalization of the results (*22*). Then, the gel was dried and exposed to a phosphoimager (Fuji Bas 1000), and the autoradiogram is shown at the top. The radioactivity was expressed as a percentage of the control after normalization by the amount of protein. (b) Everted membrane vesicles and intact cells were incubated with MTSES as described under the Materials and Methods. Proteins were purified by Ni−NTA-affinity chromatography and labeled on the beads with the fluorescent reagent NEM-fluorescein to estimate the percentage of free cysteines left. Then, the eluted proteins were resolved by SDS−PAGE, and the NEM-fluorescein labeling was determined by a phosphoimager, normalized by the respective protein concentration, and calculated as a percentage of the MTSES untreated control (100%). Accessibility to MTSES = 100% − the percentage of NEM-fluorescein labeling. White bars, in everted membrane vesicles; gray bars, in intact cells. In each experiment of labeling with MTSES, several concentrations of the reagent were tested. The standard deviation is indicated.

yielded a suppressor mutation, A130V/K300C (TMS IV/X, Figure 2a). The mutant A130V/K300C was independently isolated following chemical or PCR mutagenesis. It expressed and grew on the Na^+-selective medium at neutral pH similar to the wild type but was less efficient than the control in Li^+ at neutral pH or in Na^+ at alkaline pH (Table 3). The maximal extent of the antiport activity of the mutant with Na^+ and Li^+ was 18 and 77% of the control (data not shown), and the apparent K_M for the ions increased (68- and 25-fold, respectively, data not shown). The high apparent K_M values for the ions explain the impaired growth of the mutant on the extreme selective media (*3*). The mutant A130C/K300C was then constructed. Although expressed as well as A130V/K300C, it less efficiently suppressed the K300C phenotype (Table 3). When these suppressor mutations are taken together, they suggest the existence of a structural and/or functional interaction between TMSs IV and X at physiological pH. Nevertheless, suppressor mutations do not necessarily imply close proximity, because they can exert their effect along wide distances in the protein. Therefore,

Table 3: Double-Cys Replacements[a]

mutation	expression	growth		
		Na^+ (7)	Na^+ (8.3)	Li^+ (7)
TMSs II−X				
E78C/G295C[b]	90	+++	+++	+++
E78C/L296C	100	+++	++	−
E78C/G299C	90	+++	−	−
E78C/K300C	85	−	−	−
E78C/G303C	40	−	−	−
E78C/I304C[b]	100	+++	+++	+++
E78K/K300E	20	++	−	+
TMSs IV−X				
A127C/K300C	90	−	−	−
A130C/G295C	60	+++	+++	+++
A130C/L296C	90	+++	+++	+++
A130C/G299C	90	+++	−	+++
A130V/K300C[c]	100	+++	++	+
A130C/K300C	90	++	−	−
A130C/G303C	50	−	−	−
A130C/I304C	100	+++	+++	+++
T132C/K300C	100	−	−	−
D133C/K300C	100	−	−	−
A137C/G295C	ND[d]	+++	−	+++
A137C/L296C	ND	+++	+++	+++
A137C/G299C	60	+++	−	−
A137C/K300C	ND	−	−	−
A137C/G303C	ND	−	−	−
A137C/I304C	ND	+++	+++	+++
controls				
pCL-HAH4	100	+++	+++	+++
pBR322	−	−	−	−

[a] Growth experiments and the determination of expression were performed and presented as described in Table 2. [b] The mutants were constructed in both pCL-HAH4 and pCL-AXH3 plasmids with identical results. [c] A130V/K300C was generated in pGM36 by random mutagenesis. [d] ND = not determined.

we applied cross-linking to estimate distances between TMS IV and X, at physiological pH, and compared them to the respective distances in the crystal structure of NhaA obtained at pH 4.

In Situ Intramolecular Cross-Linking between TMSs IV and X of NhaA at Physiological pH. For the purpose of intramolecular cross-linking, we constructed double-Cys replacements, one in TMS IV and the other in TMS X (Table 3), based on the distances between the α carbons of the respective residues in the acidic pH locked NhaA structure (see ref *13* and Figure 2b). The chosen distances were between 8 and 20 Å, so that BMH [3.5−15.6 Å span (*40*)], *o*-PDM (7.7−10.5 Å span), and MTS-2-MTS (5.2 Å span) were expected to cross-link certain pairs.

Many of the double mutants expressed well (Table 3). In line with the results obtained with the single mutants, the growth phenotype of the double mutants show that K300C and G303C exert a lethal phenotype on many Cys replacements in TMS IV (Table 3) and G299C and G295C (A130C/G299C and A137C/G295C) affect the Na^+ resistance more than the Li^+ resistance (Table 3).

We next applied cross-linking on double-Cys mutants that grew on, at least, certain selective media. Note that the double-Cys replacements were each located on the opposite side of the unique trypsin cleavage site of NhaA (K249, Figure 2a). Hence, in the cross-linking protocol, the cross-linkers were applied at pH 7.5, *in situ*, on isolated membrane vesicles and then digestion with trypsin was exploited to detect changes in the mobility of the cross-linked products (*8*, *23*). For a positive control, we used the double mutant N177C/S352C that has previously been shown to cross-link very efficiently (see refs *17* and *23* and Figure 5a). In the untreated control, the resulting two tryptic products can be easily identified by SDS−PAGE as 24 and 17 kDa fragments (HF and LF fragments, respectively, lane b in Figure 5a). CL-NhaA bands at 32.5 kDa (open arrow of lane a in Figure 5a). The treatment of membrane vesicles expressing CL-NhaA by the cross-linking reagents BMH, *o*-PDM, or MTS-2-MTS had no effect on the proteolytic products of the protein (data not shown and ref *23*). Hence, these cross-linking reagents are specific to the Cys replacements in the protein. Furthermore, using these cross-linking reagents, we did not find any intermolecular cross-linking between monomers of the single or double mutants (data not shown).

The mutant pair A130C/G295C significantly cross-linked with two cross-linking reagents (BMH and *o*-PDM, Figure 5a) but not with MTS-2-MTS (data not shown), while the other pairs of mutants did not cross-link with any of the cross-linking reagents (data not shown). The lack of cross-linking in many of the double mutants cannot be ascribed to their inaccessibility (Figure 5 and ref *17*). Therefore, at pH 7.5, only the pair A130C/G295C was in the right orientation and proximity to cross-link. Hence, at both pH values 4 and 7.5, the N-terminus part of TMS X is in proximity to TMS IVp (see ref *13* and Figures 1 and 2b).

Physical and/or Functional Interaction between TMSs X and II at Physiological pH. The acid-locked structure of NhaA shows that TMS II is wide apart from helix X (see ref *13* and Figure 1). However, biochemical and genetic (*41*, *42*) evidence obtained with *Helicobacter pylori* (Hp-NhaA), a close homologue of NhaA [49% identity and 82% similarity (*1*, *41*)] has suggested functional and/or structural importance of TMSs II and X and a possible interaction between these helices. Residue K347 of Hp-NhaA aligns with K300 of Ec-NhaA and is likewise highly conserved. Similar to the results shown here with K300C of Ec-NhaA, mutations K347E and K347C in Hp-NhaA inactivated the antiporter, while K347Q resulted in an antiporter with a very low activity. Second-site mutation K347E/E87K in Hp-NhaA suppressed K347E (*33*). E87 of Hp-NhaA aligns with residue E78 in the C-terminal part of helix II of Ec-NhaA, and both are highly conserved (see ref *33* and Figures 1 and 2b). We therefore constructed the mutants K300E (Table 2), E78C/K300C, and E78K/K300E (Table 3) in Ec-NhaA. Similar to K300C, K300E was expressed but did not grow on the high Na^+- and Li^+-selective media (Table 2). Whereas both double mutants, E78C/K300C and E78K/K300E, were expressed (85 and 20% of the wild type, respectively), E78C/K300C did not grow on the selective media but K300E/E78K did grow on the Na^+-selective medium, at pH 7.0 (Table 3). The maximal antiport activity of E78K/K300E in everted membrane vesicles was 15% of the wild-type activity at 100 mM Na^+ (data not shown), implying that the apparent K_M was very high, and explains the lack of growth of the mutant on Na^+ at alkaline pH. The Li^+/H^+ antiport maximal activity in the presence of 100 mM Li^+ was 45% of the wild type, yet the apparent K_M was 97.5 mM, explaining the very weak growth on the Li^+-selective medium (Table 3). In any event, it is apparent that the mutant E78K/K300E suppresses certain phenotypes of K300E. This result suggests a structural and/

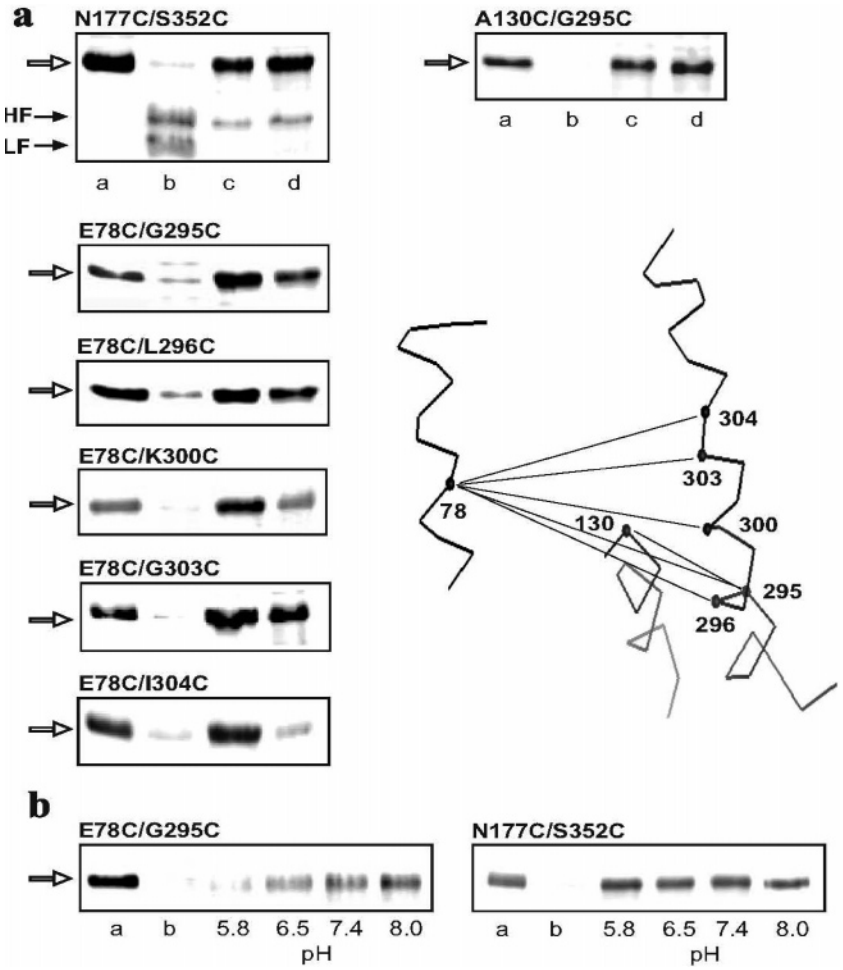

FIGURE 5: *In situ* intramolecular cross-linking in NhaA. Membrane vesicles were prepared from the TA16 strain expressing the indicated double-Cys-replacement mutants as described under the Materials and Methods. (a) Membranes were cross-linked, *in situ*, by BMH (lanes c) or *o*-PDM (lanes d) or not cross-linked (lanes b). For analysis of the cross-linked products, the Ni^{2+}−NTA-affinity-purified protein was treated at pH 8.4 with trypsin and resolved by SDS−PAGE as described under the Materials and Methods. Control samples, not treated with either the cross-linker or trypsin, are shown in lanes a. (b) Membranes of mutants N177C/S352C (positive control) and E78C/G295C were cross-linked with *o*-PDM at various pH values as indicated; otherwise, the procedure was the same as above. The experiments were repeated at least 3 times, and the results were essentially identical. HF and LF, the tryptic fragments of CL-NhaA-His_6; open arrow, intact CL-NhaA-His_6. Discussed parts of the protein are depicted by a ribbon representation for clarity purposes.

or functional interaction between helices II and X at physiological pH.

To estimate distances between E78C of helix II and helix X in Ec-NhaA, at physiological pH, the following Cys-replacement mutants were constructed in addition to E78C/K300C: E78C/G295C, E78C/L296C, E78C/G299C, E78C/G303C, and E78C/I304C (Table 3). The double mutants containing either K300C or G303C did not grow at all on the selective media. Mutants E78C/G295C and E78C/I304C grew similar to the wild type, and mutants E78C/L296C and E78C/G299C did not grow on the Li^+-selective medium but grew on the Na^+-selective medium, at least at neutral pH (Table 3).

Remarkably, BMH efficiently cross-linked all double mutants (Figure 5a). *o*-PDM was much less efficient but significantly cross-linked mutants E78C/G295C, E78C/L296C, E78C/K300C, E78C/G303C (Figure 5a), and E78C/G299C (data not shown). MTS-2-MTS did not cross-link any of the double mutants (data not shown). Hence, a large discrepancy exists between the distances spanning the respective residues of TMSs II and X in the crystal structure (pH 4) and the activated NhaA (alkaline pH). These results suggest that the respective residues change their location with pH.

To test this possibility, the cross-linking of the mutant E78C/G295C was performed at various pH values (Figure 5b). As a control, we used the mutant N177C/S352C (loops V/VI and XI/XII, Figure 2a) that has previously been shown to cross-link very efficiently (*23*). Indeed, this mutant cross-linked at all pH values between pH 5.8 and 8.0 (Figure 5b). In addition, CL-NhaA did not show any modification by NEM at any of the tested pH values (data not shown and ref *14*). In mark contrast, the cross-linking of mutant E78C/G295C was pH-dependent; it increased gradually with pH, from almost no cross-linking at pH 5.8 to very prominent cross-linking at pH 8.0. When our results are taken together, they reveal that the distance between the conserved patch of TMS X and E78C of TMS II decreases at physiological pH, implying a pH-dependent conformational pH of either one or both helices.

DISCUSSION

The newly determined 3D crystal structure of the acidic pH down-regulated NhaA provided the basis for understand-

ing the mechanism of Na^+/H^+ exchange and its unique regulation by pH (*13*). Furthermore, it paved the way to conduct structural-based studies aimed to answer questions that have remained open. These questions, in particular, are related to the open active conformation of NhaA, because in contrast to the crystal structure obtained at pH 4, activation of NhaA occurs between pH 7.0 and 8.5. In the present work, we studied the functional/structural role of TMS X in the active state of NhaA, at physiological pH, using *in silico* bioinformatics and biochemical and genetic approaches. We revealed a central conserved segment in TMS X of NhaA that contains residues that are the most important for the antiport mechanism. Strikingly, when the predictions based on the acidic pH crystal structure were challenged with the data obtained at physiological pH, we unraveled that the distance between the conserved part of helixes X and II decreases upon an alkaline pH shift, implying a pH-induced conformational change of one or both helices. We suggest that this conformational change is part of the mechanism of activation of NhaA by pH.

Cys replacement of the conserved residues in TMS X and their study at physiological pH showed that all mutants were expressed in the membrane and exhibited antiport activity that is accounted for by their growth phenotype; e.g., lack of growth or impaired growth was caused by the lack of antiport activity or a very high increase in the apparent K_M of the antiporter to the respective ions. Remarkably, a highly conserved residue (G303), located at the center of the conserved segment of helix X was found essential for Na^+ and Li^+ antiport activity. Notably, two additional NhaA mutants in the center of TMS X, L302P and G303R, have previously been claimed to lose salt resistance, although their expression level has not been determined (*43*).

Most interestingly, the mutations affected the Li^+/H^+ antiport activity less than the Na^+/H^+ antiport activity. Whereas K300C had no Na^+/H^+ antiport activity, it exhibited Li^+/H^+ antiport activity, albeit with a very high apparent K_M for Li^+ (4 mM). Similarly, whereas the apparent K_M for Na^+ of L296C and G299C was 10- and 34-fold higher than that of the control, the apparent K_M for Li^+ was unchanged or increased 8-fold, respectively. Our previous structure-based calculations have suggested that, during transport, the nonhydrated ions penetrate into the putative binding site at the bottom of the cytoplasmic funnel (*13*). However, both Na^+ and Li^+ were not resolved in the crystal structure of NhaA. Therefore, we can only speculate that the differential effect of the mutants on the ion selectivity of NhaA is due to the smaller size of the nonhydrated Li^+ ion (0.6 Å) as compared to the nonhydrated Na^+ ion (0.95 Å). In addition, as suggested previously, Li^+ requires less binding residues than Na^+ (*44*). In any event, the differential effect of the mutants on the ion selectivity implies that Cys replacements of the respective residues in helix X mainly affect the translocation and not the pH regulation. Indeed, we did not observe any effect of the mutants on the pH profile of the antiport activity, which, at saturating Na^+ concentrations, was similar to that of the wild-type antiporter (Figure 3).

Accessibility tests at pH 7.5 showed that G299C, K300C, and G303C are alkylated by NEM, a reaction that requires ionization of the Cys-sulfhydryl to its thiolate form. This occurs in the presence of water molecules. However, in membrane proteins, in the presence of a proton acceptor other than water, it is possible that the protein/protein interaction lowers the local p*K* of the Cys-sulfhydryl and the reaction takes place without water. Assuming that there is no proton acceptor other than water at this location in the molecule, our results suggest the existence of water in the vicinity of G299C, K300C, and G303C. Furthermore, accessibility tests to the negatively charged MTSES showed that these three residues are accessible from the cytoplasmic side of the membrane. Because G303C is a lethal mutant, it is possible to argue that its position is not relevant to the active conformation of NhaA. However, both K300C and G299C exhibit a significant Li^+/H^+ antiport activity at saturating Li^+ concentrations (Table 2 and data not shown). It is therefore suggested that the center of the conserved segment of TMS X that is exposed to the aqueous environment opens most likely to the cytoplasmic funnel. This suggestion has recently been strongly supported by our structure-based *in silico* approaches applied on NhaA (*45*); the protonation states of residues in NhaA in combination with the effect of explicit water molecules on the electrostatic interactions were studied by the multiconformation continuum electrostatics (MCCE) method. These calculations predicted that K300 is in contact with internal water molecules, even though water molecules were not seen crystallographically.

The structure of the acidic pH locked conformation predicts close proximity between the N terminus of helix X and the short helix IVp of the TMSs IV/XI assembly (see ref *13* and Figure 2b). As shown here, a functional and/or structural interaction also exists between these helices, at physiological pH. Thus, mutations in helix IVp (A130V and A130C) suppress certain growth and membrane phenotypes of the mutant K300C. Furthermore, scanning of helix IV and X by double-Cys replacements (one in the former and one in the latter) shows that K300C and G303C exert strong negative dominance on many residues in TMS IV, suggesting that the respective interface between these helices does not tolerate changes. Although the genetic approach highly suggests physical interactions between the respective helices, it cannot exclude the possibility that the mutants exert their effect along wide distances in the protein. However, the double mutant A130C/G295C exhibits significant chemical cross-linking at pH 7.5, by both the flexible bifunctional cross-linker BMH that can span 3.5−15.6 Å and the rigid *o*-PDM that spans 7.7−10.5 Å (*40*) but not by the short cross-linker MTS-2-MTS that spans 5.2 Å. In the acidic pH locked crystal structure, the respective distance between the α carbons of A130 and G295 is 12 Å (Figure 2b). Hence, the respective distances in the acidic pH down-regulated and active conformations of NhaA are similar.

The crystal structure of the acid pH locked conformation shows that the distances of all of the mutations (α carbons) in TMS X are at least 25 Å apart from E78 in TMS II, which is located at the orifice of the cytoplasmic funnel (see Figures 1 and 2b and ref *13*). It was therefore, most surprising to observe very efficient chemical cross-linking with the double mutants comprised of one mutation in TMS II (E78C) and the other in TMS X (G295C, L296C, G299C, K300C, G303C, and I304C). All pairs cross-linked with BMH, and many cross-linked with *o*-PDM (E78C/G295C, E78C/L296C, E78C/K300C, and E78C/G303C; Figure 5a). Except for the double mutants bearing either K300C or G303C that do not grow on the selective media, the other mutants either have

the wild-type phenotype (E78C/G295C and E78C/I304C) or are impaired in growth in the extreme selective medium (E78C/L296C and E78C/G299C). Hence, it is concluded that cross-linking cannot be ascribed to an aberrant conformation because of the mutation but rather to the active conformation of NhaA at alkaline pH. Strikingly, the cross-linking between E78C and G295C has been shown to be pH-dependent, in a manner that reflects the pH dependence of NhaA (Figures 2 and 5b). In line with the cross-linking data, we found that mutation E78K/K300E suppresses the negative growth phenotype of K300E on high Na^+-selective media (at neutral pH).

Our genetic and biochemical results are strongly supported by *in silico* MCCE and molecular dynamics (MD) simulation studies performed on NhaA at pH 4 and 8 (*45*, *48*). The MD simulation predicts a hinge at the region of K300 and P301 of helix X. In contrast to the slightly curved helix X at pH 4, it is kinked at the hinge that moves toward helix II, at alkaline pH. It should also be noted that in the crystal structure K300 has a high Debye−Huckel *B* factor, which is indicative of helix (or side-chain) mobility.

It is clear that a high-resolution crystal structure of the open active conformation of NhaA at physiological pH is required to ascertain our conclusions obtained in this study by biochemical and genetic approaches conducted at physiological pH. Nevertheless, it is remarkable that many of the biochemical/genetic data obtained at physiological pH, previously (*9*, *16*, *17*) and now, are totally consistent with predictions based on the structure of the acidic pH locked conformation of NhaA (*13*). For example, most of the distances measured by cross-linking at physiological pH (refs *17* and *23* and unpublished results) are in accordance with the distances measured in the structure of the acid pH locked conformation of NhaA (*13*). Hence, many parts of the NhaA architecture do not change with pH. It also implies that, when a result obtained at alkaline pH contradicts that obtained at acidic pH, two alternative explanations exist: (1) The resolution of the acid-locked conformation of NhaA is not high enough to detect the respective result. (2) The respective result is induced at alkaline pH. In summary, when the acidic pH-based crystal structure predictions were challenged with results obtained here by biochemical and genetic experiments conducted at physiological pH, a new pH-induced conformational change was revealed in NhaA.

ACKNOWLEDGMENT

We thank Meytal Landau and Prof. Nir Ben-Tal (Department of Biochemistry, Tel-Aviv University, Israel) for help in the evolutionary-based computational study.

REFERENCES

1. Padan, E., Venturi, M., Gerchman, Y., and Dover, N. (2001) Na^+/H^+ antiporters, *Biochim. Biophys. Acta 1505*, 144−157.
2. Padan, E., Tzubery, T., Herz, K., Kozachkov, L., Rimon, A., and Galili, L. (2004) NhaA of *Escherichia coli*, as a model of a pH-regulated Na^+/H^+ antiporter, *Biochim. Biophys. Acta 1658*, 2−13.
3. Padan, E., Bibi, E., Masahiro, I., and Krulwich, T. A. (2005) Alkaline pH homeostasis in bacteria: New insights, *Biochim. Biophys. Acta 1717*, 67−88.
4. Padan, E., Maisler, N., Taglicht, D., Karpel, R., and Schuldiner, S. (1989) Deletion of *ant* in *Escherichia coli* reveals its function in adaptation to high salinity and an alternative Na^+/H^+ antiporter system(s), *J. Biol. Chem. 264*, 20297−20302.
5. Brett, C. L., Donowitz, M., and Rao, R. (2005) Evolutionary origins of eukaryotic sodium/proton exchangers, *Am. J. Physiol. 288*, C223−C239.
6. Taglicht, D., Padan, E., and Schuldiner, S. (1991) Overproduction and purification of a functional Na^+/H^+ antiporter coded by nhaA (ant) from *Escherichia coli*, *J. Biol. Chem. 266*, 11289−11294.
7. Venturi, M., Rimon, A., Gerchman, Y., Hunte, C., Padan, E., and Michel, H. (2000) The monoclonal antibody 1F6 identifies a pH-dependent conformational change in the hydrophilic NH_2 terminus of NhaA Na^+/H^+ antiporter of *Escherichia coli*, *J. Biol. Chem. 275*, 4734−4742.
8. Gerchman, Y., Rimon, A., and Padan, E. (1999) A pH-dependent conformational change of NhaA Na^+/H^+ antiporter of *Escherichia coli* involves loop VIII−IX, plays a role in the pH response of the protein, and is maintained by the pure protein in dodecyl maltoside, *J. Biol. Chem. 274*, 24617−24624.
9. Tzubery, T., Rimon, A., and Padan, E. (2004) Mutation E252C increases drastically the K_M value for Na^+ and causes an alkaline shift of the pH dependence of NhaA Na^+/H^+ antiporter of *Escherichia coli*, *J. Biol. Chem. 279*, 3265−3272.
10. Orlowski, J., and Grinstein, S. (2004) Diversity of the mammalian sodium/proton exchanger SLC9 gene family, *Pflugers Arch. 447*, 549−565.
11. Putney, L. K., Denker, S. P., and Barber, D. L. (2002) The changing face of the Na^+/H^+ exchanger, NHE1: Structure, regulation, and cellular actions, *Annu. Rev. Pharmacol. Toxicol. 42*, 527−552.
12. Wakabayashi, S., Hisamitsu, T., Pang, T., and Shigekawa, M. (2003) Kinetic dissection of two distinct proton binding sites in Na^+/H^+ exchangers by measurement of reverse mode reaction, *J. Biol. Chem. 278*, 43580−43585.
13. Hunte, C., Screpanti, M., Venturi, M., Rimon, A., Padan, E., and Michel, H. (2005) Structure of a Na^+/H^+ antiporter and insights into mechanism of action and regulation by pH, *Nature 534*, 1197−1202.
14. Olami, Y., Rimon, A., Gerchman, Y., Rothman, A., and Padan, E. (1997) Histidine 225, a residue of the NhaA−Na^+/H^+ antiporter of *Escherichia coli* is exposed and faces the cell exterior, *J. Biol. Chem. 272*, 1761−1768.
15. Rothman, A., Padan, E., and Schuldiner, S. (1996) Topological analysis of NhaA, a Na^+/H^+ antiporter from *Escherichia coli*, *J. Biol. Chem. 271*, 32288−32292.
16. Galili, L., Rothman, A., Kozachkov, L., Rimon, A., and Padan, E. (2002) Transmembrane domain IV is involved in ion transport activity and pH regulation of the NhaA−Na^+/H^+ antiporter of *Escherichia coli*, *Biochemistry 41*, 609−617.
17. Galili, L., Herz, K., Dym, O., and Padan, E. (2004) Unraveling functional and structural interactions between transmembrane domains IV and XI of NhaA Na^+/H^+ antiporter of *Escherichia coli*, *J. Biol. Chem. 279*, 23104−23113.
18. Rimon, A., Gerchman, Y., Kariv, Z., and Padan, E. (1998) A point mutation (G338S) and its suppressor mutations affect both the pH response of the NhaA−Na^+/H^+ antiporter as well as the growth phenotype of *Escherichia coli*, *J. Biol. Chem. 273*, 26470−26476.
19. Pinner, E., Kotler, Y., Padan, E., and Schuldiner, S. (1993) Physiological role of nhaB, a specific Na^+/H^+ antiporter in *Escherichia coli*, *J. Biol. Chem. 268*, 1729−1734.
20. Davies, B., and Mingioli, E. (1950) Mutants of *Escherichia coli* requiring methionine or vitamin B_{12}, *J. Bacteriol. 60*, 17−28.
21. Karpel, R., Olami, Y., Taglicht, D., Schuldiner, S., and Padan, E. (1988) Sequencing of the gene ant which affects the Na^+/H^+ antiporter activity in *Escherichia coli*, *J. Biol. Chem. 263*, 10408−10414.
22. Gerchman, Y., Rimon, A., Venturi, M., and Padan, E. (2001) Oligomerization of NhaA, the Na^+/H^+ antiporter of *Escherichia coli* in the membrane and its functional and structural consequences, *Biochemistry 40*, 3403−3412.
23. Rimon, A., Tzubery, T., Galili, L., and Padan, E. (2002) Proximity of cytoplasmic and periplasmic loops in NhaA Na^+/H^+ antiporter of *Escherichia coli* as determined by site-directed thiol cross-linking, *Biochemistry 41*, 14897−14905.
24. Landau, M., Mayrose, I., Rosenberg, Y., Glaser, F., Martz, E., Pupko, T., and Ben-Tal, N. (2005) ConSurf 2005: The projection of evolutionary conservation scores of residues on protein structures, *Nucleic Acids Res. 33*, W299−W302.
25. Bateman, A., Coin, L., Durbin, R., Finn, R. D., Hollich, V., Griffiths-Jones, S., Khanna, A., Marshall, M., Moxon, S., Son-

nhammer, E. L., Studholme, D. J., Yeats, C., and Eddy, S. R. (2004) The Pfam protein families database, *Nucleic Acids Res. 32*, D138−D141.
26. Ho, S. N., Hunt, H. D., Horton, R. M., Pullen, J. K., Pease, L. R. (1989) Site-directed mutagenesis by overlap extension using the polymerase chain reaction, *Gene 77*, 51−59.
27. Fisher, C. L., and Pei, G. K. (1997) Modification of a PCR-based site-directed mutagenesis method, *BioTechniques 23*, 570−574.
28. Rothman, A. (1997) A study of the structure /function relation of NhaA, a sodium proton antiporter from *E. coli*, Ph.D. Thesis, Hebrew University of Jerusalem, Jerusalem, Israel.
29. Supek, F., Supekova, L., and Nelson, N. (1994) Features of vacuolar H^+-ATPase revealed by yeast suppressor mutants, *J. Biol. Chem. 269*, 26479−26485.
30. Rosen, B. P. (1986) Ion extrusion systems in *E. coli*, *Methods Enzymol. 125*, 328−386.
31. Goldberg, E. B., Arbel, T., Chen, J., Karpel, R., Mackie, G. A., Schuldiner, S., and Padan, E. (1987) Characterization of a Na^+/H^+ antiporter gene of *Escherichia coli*, *Proc. Natl. Acad. Sci. U.S.A. 84*, 2615−2619.
32. Schuldiner, S., and Fishkes, H. (1978) Sodium-proton antiport in isolated membrane vesicles of *Escherichia coli*, *Biochemistry 17*, 706−711.
33. Tsuboi, Y., Inoue, H., Nakamura, N., and Kanazawa, H. (2003) Identification of membrane domains of the Na^+/H^+ antiporter (NhaA) protein from *Helicobacter pylori* required for ion transport and pH sensing, *J. Biol. Chem. 278*, 21467−21473.
34. Padan, E., Venturi, M., Michel, H., and Hunte, C. (1998) Production and characterization of monoclonal antibodies directed against native epitopes of NhaA, the Na^+/H^+ antiporter of *Escherichia coli*, *FEBS Lett. 441*, 53−58.
35. Gerchman, Y., Olami, Y., Rimon, A., Taglicht, D., Schuldiner, S., and Padan, E. (1993) Histidine-226 is part of the pH sensor of NhaA, a Na^+/H^+ antiporter in *Escherichia coli*, *Proc. Natl. Acad. Sci. U.S.A. 90*, 1212−1216.
36. Bradford, M. M. (1976) A rapid and sensitive method for the quantitation of microgram quantities of protein utilizing the principle of protein−dye binding, *Anal Biochem. 72*, 248−254.
37. Ninio, S., Elbaz, Y., and Schuldiner, S. (2004) The membrane topology of EmrE−A small multidrug transporter from *Escherichia coli*, *FEBS Lett. 562*, 193−196.
38. Akabas, M. H., Stauffer, D. A., Xu, M., and Karlin, A. (1992) Acetylcholine receptor channel structure probed in cysteine-substitution mutants, *Science 258*, 307−310.
39. Akabas, M. H., Kaufmann, C., Archdeacon, P., and Karlin, A. (1994) Identification of acetylcholine receptor channel-lining residues in the entire M2 segment of the α subunit, *Neuron 13*, 919−927.
40. Green, N. S., Reisler, E., and Houk, K. N. (2001) Quantitative evaluation of the lengths of homobifunctional protein cross-linking reagents used as molecular rulers, *Protein Sci. 10*, 1293−1304.
41. Inoue, H., Tsuboi, Y., and Kanazawa, H. (2001) Chimeric Na^+/H^+ antiporters constructed from NhaA of *Helicobacter pylori* and *Escherichia coli*: Implications for domains of NhaA for pH sensing, *J. Biochem. 129*, 569−576.
42. Kuwabara, N., Inoue, H., Tsuboi, Y., Nakamura, N., and Kanazawa, H. (2004) The fourth transmembrane domain of the *Helicobacter pylori* Na^+/H^+ antiporter NhaA faces a water-filled channel required for ion transport, *J. Biol. Chem. 279*, 40567−40575.
43. Noumi, T., Inoue, H., Sakurai, T., Tsuchiya, T., and Kanazawa, H. (1997) Identification and characterization of functional residues in a Na^+/H^+ antiporter (NhaA) from *Escherichia coli* by random mutagenesis, *J. Biochem. 121*, 661−670.
44. Kaim, G., Wehrle, F., Gerike, U., and Dimroth, P. (1997) Molecular basis for the coupling ion selectivity of F1F0 ATP synthases: Probing the liganding groups for Na^+ and Li^+ in the c subunit of the ATP synthase from *Propionigenium modestum*, *Biochemistry 36*, 9185−9194.
45. Olkhova, E., Hunte, C., Screpanti, E., Padan, E., and Michel, H. (2006) Multiconformation continuum electrostatics analysis of the NhaA Na^+/H^+ antiporter of *Escherichia coli* with functional implications, *Proc. Natl. Acad Sci. U.S.A. 103*, 2629−2634.
46. Kraulis, P. J. (1991) MOLSCRIPT: A program to produce both detailed and schematic plots of protein structures, *J. Appl. Crystallogr. 24*, 946−950.
47. Merritt, E. A., and Bacon, D. J. (1997) Raster3D photorealistic molecular graphics, *Methods Enzymol. 277*, 505−524.
48. Olkhova, E., Padan, E., and Michel, H. (2007) The influence of protonation states on the dynamics of the NhaA Na^+/H^+ antiporter from *Escherichia coli*, *J. Biophys.*, in press.

BI602393S